Available online at www.sciencedirect.com
SCIENCE DIRECT
ELSEVIER
European Journal of Mechanics B/Fluids 23 (2004) 815–833
EUROPEAN JOURNAL OF MECHANICS B/FLUIDS

On Tollmien–Schlichting-like waves in streaky boundary layers

Carlo Cossu [a,*], Luca Brandt [b]

[a] *Laboratoire d'hydrodynamique (LadHyX), CNRS–École polytechnique, 91128 Palaiseau cedex, France*
[b] *KTH Mechanics, 10044 Stockholm, Sweden*

Received 5 August 2003; received in revised form 30 April 2004; accepted 4 May 2004

Available online 29 July 2004

Abstract

The linear stability of the boundary layer developing on a flat plate in the presence of finite-amplitude, steady and spanwise periodic streamwise streaks is investigated. The streak amplitudes considered here are below the threshold for onset of the inviscid inflectional instability of sinuous perturbations. It is found that, as the amplitude of the streaks is increased, the most unstable viscous waves evolve from two-dimensional Tollmien–Schlichting waves into three-dimensional varicose fundamental modes which compare well with early experimental findings. The analysis of the growth rates of these modes confirms the stabilising effect of the streaks on the viscous instability and that this stabilising effect increases with the streak amplitude. Varicose subharmonic modes are also found to be unstable but they have growth rates which typically are an order of magnitude lower than those of fundamental modes. The perturbation kinetic energy production associated with the spanwise shear of the streaky flow is found to play an essential role in the observed stabilisation. The possible relevance of the streak stabilising role for applications in boundary layer transition delay is discussed.

1. Introduction

1.1. Streaky boundary layers

In the absence of external perturbations or wall imperfections, the boundary layer developing on a flat plate is spanwise uniform (two-dimensional) and is well described by the Blasius similarity solution (see, e.g., [1]). In the two-dimensional boundary layer, however, small amounts of streamwise vorticity are very effective in pushing low momentum fluid away from the wall and high momentum fluid towards the wall eventually leading to large elongated spanwise modulations of the streamwise velocity called streamwise streaks. The mechanism of streak generation, described above and known as the 'lift-up effect' [2], is based on an inviscid process and applies to shear flows in general [3]. The effect of viscosity eventually dominates rendering the growth of the streaks, which however is of the order of the Reynolds number [4,5], only transient. The potential of shear flows to exhibit such large transient growths is related to the non-normal nature of the linearised stability operator (for a review the reader may refer to the book by Schmid and Henningson [6]). The most dangerous perturbations, leading to the 'optimal transient growths', have been found to consist of streamwise vortices and have been computed for a number of shear flows. In flat plate boundary layers, the most amplified perturbations have spanwise scales of the order of the boundary layer thickness [7,8]. The effect of vorticity on a boundary layer is also investigated in Choudhari [9], wherein it was demonstrated that three-dimensional gusts can excite boundary layer motions that resemble the streaks due to weak free-stream turbulence. Bertolotti [10] studied the receptivity to streamwise vortices in the free stream in a linear region excluding the leading edge,

* Corresponding author.
E-mail address: carlo.cossu@ladhyx.polytechnique.fr (C. Cossu).

0997-7546/$ – see front matter
doi:10.1016/j.euromechflu.2004.05.001

while Wundrow and Glodstein [11] (see references therein) considered the effect of incoming vorticity by means of asymptotic expansions.

Streamwise streaks are therefore expected to appear whenever a boundary layer is exposed to perturbations with streamwise and wall-normal vorticity in the incoming free stream. An extensively studied case is the boundary layer developing in the presence of free-stream turbulence. In early observations, Dryden [12] and Taylor [13] reported that spanwise modulations of the boundary layer thickness are generated in the presence of free-stream turbulence. These observations were confirmed and further detailed by, among others, Arnal and Juillen [14] and Kendall [15] who coined the term 'Klebanoff modes' for the observed streaks, referring to early observations by Klebanoff [16]. The streaks forced by free-stream turbulence typically slowly oscillate in the boundary layer in a random way. Streamwise streaks may also be forced by streamwise vortices artificially generated in the free stream (e.g. [17]), by blowing and suction at the wall (e.g. [18]) or by wall-roughness elements (e.g. [19,20]).

1.2. Stability of streaky boundary layers

In the absence of streaks the (two-dimensional) Blasius boundary layer is linearly stable to inviscid perturbations. Prandtl [21] suggested that viscosity may, contrary to intuition, lead to instability if the work of the Reynolds stress, generated by viscous modes, against the wall-normal shear is positive and exceeds the viscous dissipation. Based on approximate solutions of the Orr–Sommerfeld equation, Tollmien [22] was then able to predict linear (viscous) instability of the Blasius boundary layer when the Reynolds number exceeds a critical value later refined by Schlichting [23]. These linear stability predictions were later confirmed by the celebrated experiments of Schubauer and Skramstad [24] who, by periodically vibrating a ribbon in the boundary layer, were able to observe unstable Tollmien–Schlichting (TS) waves. As TS waves grow to amplitudes of the order of 1% of the free-stream velocity, secondary instability sets in (for a review see Herbert [25]), eventually leading to breakdown and transition to turbulence. This scenario is today well understood and often referred to as the 'classical' transition scenario of boundary layers in a low noise environment.

In the case of streaky boundary layers, the streamwise velocity profiles develop inflection points which may support inviscid instabilities for sufficiently large streak amplitudes. For the optimal streaks considered here, it has been found [26] that the critical streak amplitude for the onset of inflectional instabilities is 26% of the free-stream velocity U_∞. Sinuous modes are the first to become unstable. The sinuous transition scenario is documented in Brandt and Henningson [27]. The experiments of boundary layer transition under free-stream turbulence by Matsubara and Alfredsson [28] seem to suggest that the breakdown to turbulence is indeed caused by high-frequency secondary instabilities of the streaks. However, Jacobs and Durbin [29] could not clearly identify such secondary instabilities from their numerical simulations. Schoppa and Hussain [30] showed that steady streaks in channel flows, stable to linear disturbances, can undergo a sinuous breakdown to turbulence if subjected to a spanwise velocity perturbation of the order of few percents of the centreline velocity. The breakdown is characterised by structures identical to those identified by Brandt and Henningson [27] in the case of a linearly unstable streak. The simulations by Brandt et al. [31] and Brandt [32] show that the characteristic structures of the spot precursors in boundary layers subject to free-stream turbulence are very similar to those observed in previous model studies on the secondary instability of steady symmetric streaks, both for the sinuous and the varicose symmetry (see Asai et al. [33] for a recent experimental investigation). The authors conclude that the breakdown is related to local instabilities driven by the strong shear layers associated with the streaks. They also note the importance of the interaction between the low- and high-speed streaks, and, consequently, of the streak motions and unsteadiness in triggering the breakdown to turbulence (see also Wu and Choudhari [34]).

In the quest for other possible transition mechanisms in streaky boundary layers, the development of the TS waves in the presence of streaks and their interaction have been studied in the past (for a review see Reed and Saric [35]). Most of the attention has been focused on possible destabilising resonances between TS waves and streaks of the same order. In particular, the nonlinear interaction of finite amplitude TS waves with streaks received most of the attention (starting with Tani and Komoda [17], and Komoda [36], and many others thereafter). Streaks may, however, reach finite amplitude before the TS waves and therefore a preliminary step should be to consider the streaky boundary layer as a three-dimensional basic flow in which linear three-dimensional waves develop. Only a few investigations, essentially experimental, concerning this linear growth phase are currently available, as summarised below.

Tani and Komoda [17] considered the development of viscous waves in a streaky boundary layer. Small wings located outside the boundary layer were used to generate steady streamwise vortices which, upon entering the boundary layer, led to the development of steady spanwise periodic modulations of its thickness, i.e. to steady streamwise streaks. A ribbon was then vibrated in the boundary layer at the frequency and Reynolds number where unstable TS waves exist in the two-dimensional Blasius boundary layer (to which we refer from here on, as Blasius-TS waves). For small ribbon vibration amplitudes, three-dimensional waves were detected with mode shapes similar to the Blasius-TS waves but with a distinct two-peak (or M-shaped) structure in the *rms* streamwise perturbation velocity near the wall in the low speed region. Unfortunately, no explicit measure of the growth rates of such waves was provided.

Kachanov and Tararykin [18] generated streamwise steady streaks by blowing and suction at the wall and used a vibrating ribbon to generate TS-type waves. They found three-dimensional waves having essentially the same phase speed as the Blasius-TS waves and with essentially the same M-shaped structure observed by Tani and Komoda [17]. Surprisingly, however, these streaky-TS waves did not amplify as they would have done in the absence of the streaks in the same parameter range.

Arnal and Juillen [14] detected 'natural' (not forced) TS-type waves riding on the unsteady streaks induced by free-stream turbulence. Grek et al. [37] and Boiko et al. [38] forced TS waves with a vibrating ribbon in a boundary layer exposed to free-stream turbulence. Using refined wave detection techniques they found unstable streaky-TS waves, which were, however, less amplified than Blasius-TS waves. These streaky-TS waves had a phase speed and shapes very similar to Blasius-TS waves. Boiko et al. [38] attributed the growth rate defect to the stabilising role of the two-dimensional averaged basic flow distortion induced by the streaks; however, they also found that a mere two-dimensional stability analysis of the average velocity profile was unable to predict a correct growth rate.

Based on perturbation expansions valid in the limit of large ratios of the streak spanwise scale to the boundary layer thickness, Wu and Luo [39] predict, for small streak amplitudes, the existence of 'modified TS waves' having a growth rate larger than the Blasius-TS waves. In this approximation, however, the effect of the spanwise shear is negligible to the leading order. The modified TS-waves analysed by the latter authors correspond to localised distortions in the base flow, while spanwise periodic perturbations have been considered by Goldstein and Wundrow [40]. On the other hand, using temporal and spatial numerical simulations, the present authors (Cossu and Brandt [41], from now on referred as CB), found that steady streaks of sufficiently large amplitude are able to reduce the linear growth of viscous instabilities up to their complete stabilisation. Further, a recent study by Kogan and Ustinov [42], appeared during the revision of the present article, shows the possibility of increasing the boundary layer stability by means of a spanwise-periodic stationary mass force distributed in the streamwise direction. This force generates a transverse flow which results in the appearance of streaks. These authors show that the suppression of unstable disturbances can increase the laminar-flow interval by 3–4 times.

1.3. Aim of the present study

The results presented in CB were limited to fundamental modes and to one single Reynolds number; only a heuristic explanation was given for the observed stabilisation and no detailed analysis of the most unstable perturbations was provided. It is therefore not clear if the phenomenon observed by CB is the same experimentally observed, for instance, by Tani and Komoda [17] and Kachanov and Tararykin [18]. Furthermore, results of CB would be in contradiction with those of Wu and Luo [39] if it is not proven that the stabilising action of the streaks observed by CB relies on the basic flow spanwise shear, absent from the long-wavelength analysis in Wu and Luo [39].

The aim of the present article is therefore: (a) to compute the shape and phase speed of the most unstable linear viscous modes living in streaky boundary layers to allow comparison with previous experimental results; (b) to analyse analogies and differences between these modes and the well known Tollmien–Schlichting waves developing in the absence of streaks; (c) to analyse the energy production and dissipation for the most unstable waves, elucidating the role played by the streak spanwise shear on the stabilisation mechanism; (d) to compute neutral stability curves of the whole streaky boundary layers therefore quantifying for the first time the streamwise extension of the streak stabilising action; (e) to check the stability of subharmonic modes, neglected in CB. This analysis enables us also to obtain the critical modes, necessary in view of the weakly nonlinear analysis of finite amplitude waves developing in the streaky boundary.

We therefore implement a linear temporal viscous stability analysis based on the extension of the classical Orr–Sommerfeld and Squire equations to basic flows which are non-uniform in the spanwise direction. The same kind of three-dimensional stability analysis, summarised by Schmid and Henningson [6], has already been applied to analyse the secondary, inflectional type, instability of streaks induced by Görtler vortices in the inviscid [43] and viscous approximation [44,45], of finite amplitude streaks developing in Couette [46] and Poiseuille [47] flows. We consider both sinuous and varicose symmetries of the perturbations for low and large amplitude streaks. Sinuous modes, however, have been found unstable only to inflectional type instabilities for large amplitude streaks with eigenfuctions and growth rates closely matching those computed in the inviscid approximation by Andersson et al. [26]. We therefore present only the results concerning streaks of intermediate amplitude, stable to inflectional instabilities, and discuss only the varicose modes, the sinuous modes being stable for the streaks under consideration. The linear stability analysis of viscous waves in spanwise modulated boundary layers is thus provided here. The streaky basic flows that we will consider result, as in Andersson et al. [26], from the nonlinear evolution of the linear spatial optimal perturbations.

The article is organised as follows. In Section 2 we describe the streaky basic flows. In Section 3 we introduce the equations and the parameters governing the temporal stability of the three-dimensional basic flows to viscous perturbations and briefly recall the definition of the perturbation kinetic energy production and dissipation. The numerical results are presented in Section 4. In particular, the effect of the streak amplitude and of the Reynolds number on the stability and energy production and

dissipation are described. In the same section we discuss the stability of the whole streaky boundary layers and the implications for transition delay. The main results are summarised in Section 5.

2. Basic flows

Following the standard boundary layer approach, we define the reference length $\bar{L}$ and the corresponding Reynolds number $Re_L = \bar{L}\overline{U}_\infty/\bar{\nu}$, where $\bar{\nu}$ is the fluid kinematic viscosity, $\overline{U}_\infty$ is the free-stream velocity and dimensional quantities are denoted by $\bar{}$. The boundary layer reference scale is defined as $\bar{\delta}_L = (\bar{L}\nu/\overline{U}_\infty)^{1/2}$. At the streamwise station $\overline{X}$, a local Reynolds number $Re_X = \overline{X}\overline{U}_\infty/\bar{\nu}$ and characteristic boundary layer reference scale $\bar{\delta}_X = (\overline{X}\nu/\overline{U}_\infty)^{1/2}$ are also defined. The streamwise, wall-normal and spanwise variables are denoted $(\overline{X}, \bar{y}, \bar{z})$, with corresponding velocities $(\overline{U}, \overline{V}, \overline{W})$. The streamwise coordinate and velocity component are respectively made dimensionless with $\bar{L}$ and $\overline{U}_\infty$, while $(\bar{y}, \bar{z})$ and $(\overline{V}, \overline{W})$ are respectively made dimensionless with $\bar{\delta}_X$ and $\overline{U}_\infty Re_X^{-1/2}$.

In the framework of the linearised boundary layer equations Andersson et al. [7] and Luchini [8] computed the optimal perturbations that, applied at the flat plate leading edge, lead to the maximum perturbation energy at the reference downstream distance $\bar{L}$. The task was not straightforward due to the non-parallel nature of the boundary layer equations and to their singularity at the leading edge. In the large Re_L limit, the optimal perturbations consisted in streamwise vortices and the most amplified disturbances in streamwise streaks. In both studies steadiness and spanwise periodicity were assumed; the optimal spanwise wavenumber, scaled on $\bar{\delta}_L$, was found to be $\beta_{\text{opt}} = 0.45$. Due to the large growth of the streaks, however, nonlinear terms soon come into play even for very small amplitudes of the streamwise optimal vortices. The effect of nonlinear terms is to quasi-saturate the streamwise energy growth and to move slightly upstream the location of maximum streak amplitude.

Closely following Andersson et al. [26] and CB, we consider as basic flows zero-pressure-gradient boundary layers on a flat plate with steady, nonlinear, spanwise periodic streaks generated by forcing 'linearly-optimal' perturbations of different amplitudes at the leading edge. The assumed spanwise wavenumber is the optimal one $\beta_{\text{opt}} = 0.45$. A set of nonlinear streaks is computed following the procedure of Andersson et al. [26] in which the linear optimal velocity field, obtained in Andersson et al. [7], is given as inflow at $X = \overline{X}/\bar{L} = 0.4$ and its nonlinear development is computed up to $X = 6$ by integrating the Navier–Stokes equations with the pseudo-spectral code described in Lundbladh et al. [48]. Such a long computational domain is obtained by following the spatial evolution of the inflow perturbations with two computational boxes. Their dimensions and the corresponding numerical resolutions are reported in Table 1. The Reynolds number in the simulations was set to be $Re_L = 185\,185$ where $\bar{L}$ (or $X = 1$) coincides with the position of optimal linear growth (see the comment below on the Reynolds number independence of the basic flows). The first computational domain (B1 in the table) has the inlet at $X = 0.4$, corresponding to $Re_X = 74\,193$. This first domain allows us to follow the perturbation up to $X = 3$. To further extend the computations and follow the streak viscous decay, the second computational box is used. Its inflow is at $X = 2.63$, corresponding to $Re_X = 486\,750$. The inflow condition is the full velocity field from the simulations with the first box.

Different indicators may be introduced to measure the streak amplitude. Tani and Komoda [17] defined the relative spanwise variation of the local displacement thickness

$$T(X) = \frac{\max_z \delta^*(X,z) - \min_z \delta^*(X,z)}{\min_z \delta^*(X,z)}, \tag{1}$$

with

$$\delta^*(X,z) = \int_0^\infty \big[1 - U(X,y,z)\big]\,\mathrm{d}y. \tag{2}$$

Table 1
Dimensions of the computational domain and resolution for the simulations performed to generate the streaky basic flows. The box dimensions are made dimensionless with respect to δ_L, the Blasius lenght scale at the position of optimised linear growth $Re_L = 185\,185$. The spanwise extension of the domain corresponds to one wavelength of the optimally growing streaks and the spanwise collocation points are extended across the full wavelength

Simulation	Inlet Re_X	Box dimensions (δ_L)	Collocation points
B1	74 193	$1228 \times 21.77 \times 13.97$	$576 \times 65 \times 32$
B2	486 750	$2509 \times 42.38 \times 13.97$	$576 \times 97 \times 32$

Andersson et al. [26] used an indicator based on a local maximum of the streamwise velocity deviation $\Delta U(X, y, z) = U(X, y, z) - U_B(X, y)$ from the Blasius profile $U_B(X, y)$:

$$A_s(X) = \frac{1}{2}\Big[\max_{y,z} \Delta U(X, y, z) - \min_{y,z} \Delta U(X, y, z)\Big], \tag{3}$$

to which they correlated the appearance of inflectional instabilities. The threshold amplitude was found to be $A_s = 0.26$. Note however that the analysis of the neutral conditions in Andersson et al. [26] was limited to the streak profiles extracted at the streamwise station $X = 2$. During the present study it has been found that unstable subharmonic sinuous modes may occur also for $A_s = 0.235$. This lower critical value is obtained considering the streak at $X = 2.75$. Here, we will consider only streaks stable to inflectional sinuous instabilities. Another indicator of the intensity of the streaks, used to optimise their linear growth in the large Reynolds number limit [8], is given by the local integral of the streamwise velocity deviation:

$$E_U(X) = \left[\frac{1}{\lambda_z}\int_0^{\lambda_z}\int_0^{\infty} \big(\Delta U(X, y, z)\big)^2 \,\mathrm{d}y\,\mathrm{d}z\right]^{1/2}. \tag{4}$$

We will consider four basic flows, denoted by A, B, C and D and listed in Table 2, corresponding to four increasing amplitudes of the upstream forcing. Case A is nothing but the Blasius boundary layer without streaks, while case D roughly represent the limit case before secondary inflectional instability. The streamwise evolution of streak amplitudes $T(X)$, $A_s(X)$ and $E_U(X)$ is

Table 2
Streak amplitude A_s for the computed basic flows. Case A corresponds to the Blasius boundary layer. Cases B, C and D are obtained increasing the amplitude of the upstream forcing

Case	Inlet A_s	Maximum A_s	A_s at $X = 2$
A	0.0000	0.0000	0.0000
B	0.0618	0.1400	0.1396
C	0.0927	0.2018	0.2017
D	0.1158	0.2432	0.24317

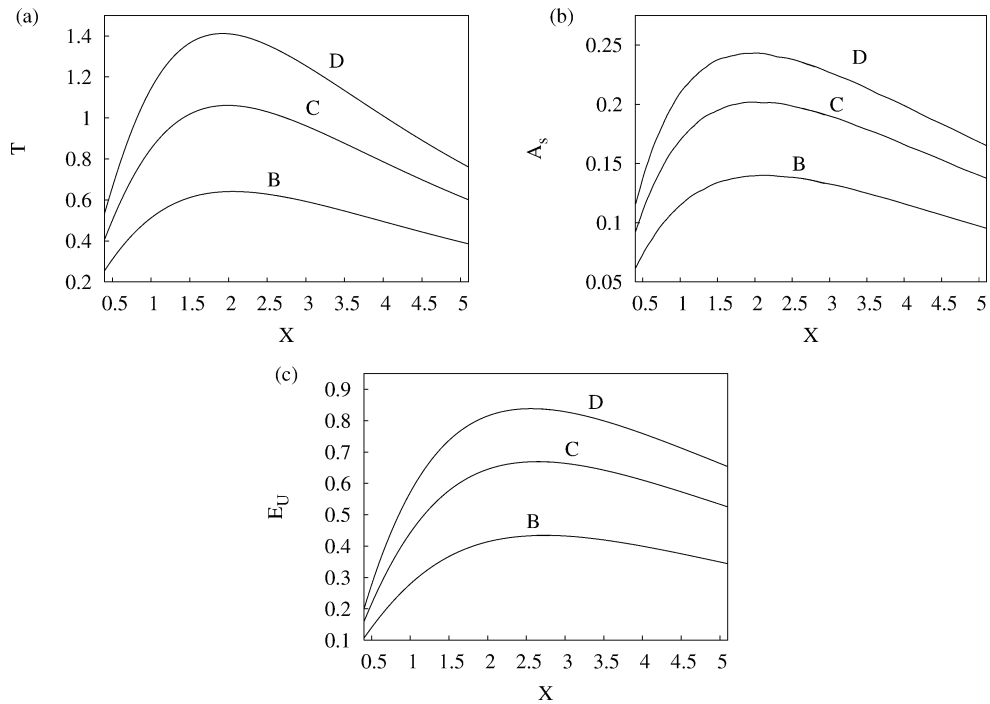

Fig. 1. Streamwise evolution of the different indicators used to define the amplitude of streaks in the computed basic flows: (a) $T(X)$, (b) $A_s(X)$ and (c) $E_U(X)$.

displayed in Fig. 1. The $T(X)$ and $A_s(X)$ measures are very similar and give essentially the same information. The maximum of the streak amplitude, for both indicators $T(X)$ and $A_s(X)$ is reached at roughly $X = 2$. The $E_U(X)$ measure is more sensitive to the boundary layer growth and gives a maximum of the streak amplitude around $X = 2.7$, which is the station where the maximum energy of the linear optimal streaks is attained Andersson et al. [7]. Streamwise velocity contour plots in the cross-stream (y, z) plane are depicted in Fig. 2 for the basic flows under consideration at $X = 2$. Note that the streaks are symmetric about the $z = 0$ axis, which is situated in the low speed region. One clearly observes how the increase of the amplitude leads to stronger variations in the boundary-layer thickness across the spanwise wavelength of the streak. The cross-plane profiles of the wall-normal $\partial U/\partial y$ and spanwise $\partial U/\partial z$ streamwise velocity gradients of streak C at $X = 2$ (cf. Fig. 2(c)) are reported in Fig. 3. The maximum of the wall-normal shear is found in the near-wall high-speed region of the streak, while the maximum spanwise velocity gradient is located in the middle of the boundary layer, in the flanks of the low-speed region.

It is worth introducing a scaling property of the considered nonlinear streaks which will be used to perform stability calculation of the streaky basic flows for a wide range of Reynolds numbers and related spanwise wave numbers. It is in fact shown in Andersson et al. [26] that a streak family $U(X, y, z)$, defined by the upstream amplitude A_0 and by the spanwise wavenumber β_0, obeys the boundary layer equations and it is therefore independent of the Reynolds number. This results in a

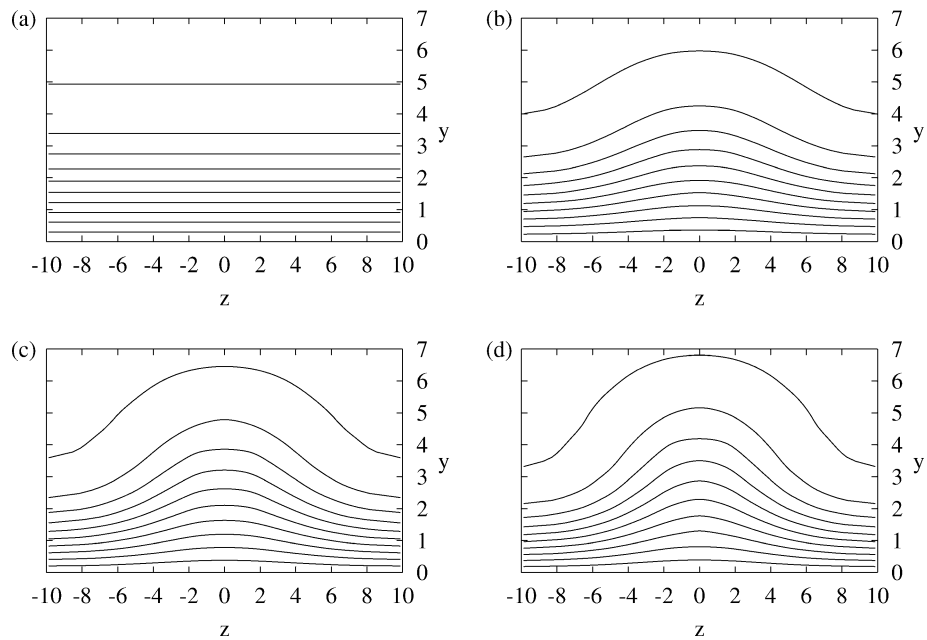

Fig. 2. Contour plot of the streamwise velocity profile $U(y, z)$ at $X = 2$ for (a) the Blasius boundary layer (case A), and for the streaky flows of increasing amplitude B, C, and D (respectively (b), (c), (d)). The contours levels $0.1, 0.2, \ldots, 0.9, 0.99$ are the same in all the plots. The y- and z-coordinates are expressed in $\bar{\delta}_X$ units.

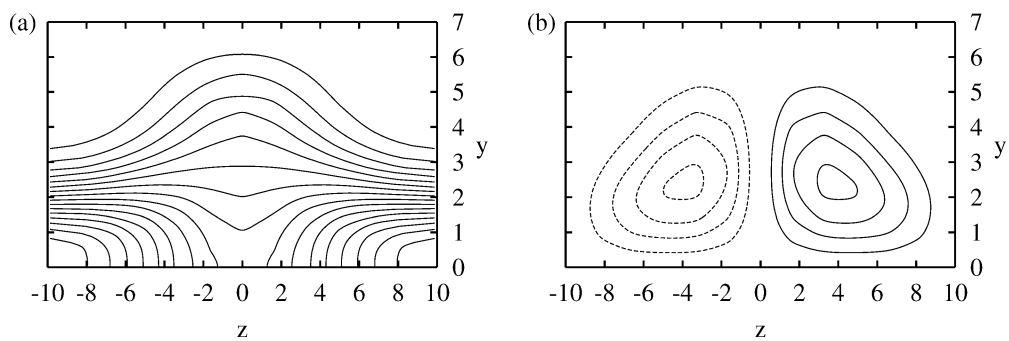

Fig. 3. Contour plot of (a) the wall-normal shear $\partial U/\partial y$ and (b) the spanwise shear $\partial U/\partial z$ at $X = 2$ for the streaky flow C. The contour spacing is 0.05 in both plots. In (a) the maximum contour levels are at the lower corners (high-speed region) and correspond to $\partial U/\partial y = 0.8$. In (b) the inner positive and negative contours correspond to $\partial U/\partial z = \pm 0.2$. The y- and z-coordinates are expressed in $\bar{\delta}_X$ units.

scaling property that couples the streamwise and spanwise scales, implying that the same solution is valid for every combination of X and β such that the product $X\beta^2$ stays constant. In other words, it is possible to freely choose the local Reynolds number pertaining to a given streak profile $U(y,z)$ extracted at any station X. This amounts to moving along the plate and varying the spanwise wavenumber β_0 so that the local spanwise wavenumber $\beta_0\delta/\delta_0$ remains constant (see also Brandt et al. [49]).

3. Formulation of the stability analysis

3.1. Governing equations

The stability analysis of the streaky basic flows is performed under a set of standard simplifying assumptions. The streaky flows satisfy the boundary layer approximation according to which variations of the streamwise velocity $\overline{U}$ with $\overline{X}$ are very slow, and the (dimensional) wall-normal and spanwise velocity components $\overline{V}$ and $\overline{W}$ are very small (of order $Re_X^{-1/2}$), compared to $\overline{U}$. It is therefore justified to analyse the local stability of the streaks by considering, at each streamwise station $\overline{X}$, the parallel flow obtained by 'freezing' the local streamwise velocity profile $\overline{U}(\overline{X},\bar{y},\bar{z})$ and neglecting the $\overline{V}$ and $\overline{W}$ velocity components. Exactly the same assumptions are made to analyse the viscous instability of the two-dimensional Blasius flow in the so called 'parallel flow approximation' (see, e.g., Drazin and Reid [50], the inviscid instability of streaky basic flows [43,26] and the viscous instability of Görtler vortices [44,45]. We therefore proceed to linearise the Navier–Stokes equations about the parallel basic flow $(U(X,y,z),0,0)$. In this context, X must be considered as a parameter and not as the current streamwise coordinate, which we call instead x. The linearised equations for the perturbation velocity components u', v', w' and pressure p' read:

$$\begin{aligned}
&u'_x + v'_y + w'_z = 0,\\
&u'_t + Uu'_x + U_y v' + U_z w' = -p'_x + (1/R)\nabla^2 u',\\
&v'_t + Uv'_x = -p'_y + (1/R)\nabla^2 v',\\
&w'_t + Uw'_x = -p'_z + (1/R)\nabla^2 w',
\end{aligned} \tag{5}$$

where all the velocities have been rescaled with $\overline{U}_\infty$ and all the lengths with the local boundary layer thickness $\bar{\delta}_X$. The local Reynolds number based on $\bar{\delta}_X$ is defined by $R = \overline{U}_\infty\bar{\delta}_X/\bar{\nu} = Re_X^{1/2}$. To allow easy comparisons of the results, we also introduce the Reynolds number based on the local displacement thickness of the Blasius boundary layer in the absence of streaks $R_{\delta^*} = 1.72R$. Homogeneous Dirichlet boundary conditions on u', v' and w' are enforced at the wall and in the free stream. The linearised Navier–Stokes equations (5) may be reduced in a straightforward way [46,6] to a system for the wall-normal perturbation velocity v' and the wall-normal perturbation vorticity $\eta' = u'_z - w'_x$:

$$\begin{aligned}
&\nabla^2 v'_t + \big(U\nabla^2 + U_{zz} - U_{yy}\big)v'_x + 2U_z v'_{xz} - (1/R)\nabla^4 v' - 2U_z w'_{xy} - 2U_{yz} w'_x = 0,\\
&\eta'_t + U\eta'_x - (1/R)\nabla^2\eta' - U_z v'_y + U_{yz} v' + U_y v'_z + U_{zz} w' = 0,
\end{aligned} \tag{6}$$

where w' may be eliminated by using the equation

$$w'_{xx} + w'_{zz} = -\eta'_x - v'_{yz}. \tag{7}$$

Homogeneous boundary conditions hold at the wall and in the free stream for v', v'_x, η' and w'. Solutions to the system (6) are sought in the form of normal modes

$$[v',\eta',w'] = \big[\hat{v}(y,z),\hat{\eta}(y,z),\widehat{w}(y,z)\big]\,\mathrm{e}^{\mathrm{i}(\alpha x-\omega t)} + \text{c.c.}, \tag{8}$$

where α is the streamwise wavenumber, ω the circular frequency, $\mathrm{i} = \sqrt{-1}$ and c.c. stands for 'complex conjugate'. The complex phase speed is defined by $c = \omega/\alpha$; the wave phase speed is given by the real part of c. The following system, which extends the usual Orr–Sommerfeld–Squire formulation to parallel spanwise non-uniform basic flows, is thus obtained:

$$\begin{aligned}
&\big[-\mathrm{i}\omega\widehat{\nabla}^2 + \mathrm{i}\alpha\big(U\widehat{\nabla}^2 + U_{zz} - U_{yy}\big) + 2\mathrm{i}\alpha U_z D_z - (1/R)\widehat{\nabla}^4\big]\hat{v} - 2\mathrm{i}\alpha(U_z D_y + U_{yz})\widehat{w} = 0,\\
&\big[-\mathrm{i}\omega + \mathrm{i}\alpha U - (1/R)\widehat{\nabla}^2\big]\hat{\eta} + (U_{yz} - U_z D_y)\hat{v} + (U_y D_z + U_{zz})\widehat{w} = 0,
\end{aligned} \tag{9}$$

with the additional identity

$$\big(D_{zz} - \alpha^2\big)\widehat{w} = -\mathrm{i}\alpha\hat{\eta} - D_y D_z\hat{v}, \tag{10}$$

where $D_y = \partial/\partial y$, $D_z = \partial/\partial z$ and $\widehat{\nabla}^2 = D_{yy} + D_{zz} - \alpha^2$. Homogeneous boundary conditions hold at the wall and in the free stream for $\hat{v}$, $\hat{v}_x$, $\hat{\eta}$ and $\widehat{w}$. Eq. (10) can be used to eliminate $\widehat{w}$ from the system (9) which can then be recast in a standard generalised eigenvalue problem.

Due to the spanwise periodicity of the basic flow, the following Floquet expansion may be applied to the normal modes (see, e.g., Schmid and Henningson [6]):

$$\hat{v}(y,z) = \mathrm{e}^{\mathrm{i}\gamma\beta_0 z} \sum_{k=-\infty}^{\infty} \tilde{v}_k(y)\,\mathrm{e}^{\mathrm{i}k\beta_0 z}; \qquad \hat{\eta}(y,z) = \mathrm{e}^{\mathrm{i}\gamma\beta_0 z} \sum_{k=-\infty}^{\infty} \tilde{\eta}_k(y)\,\mathrm{e}^{\mathrm{i}k\beta_0 z}, \tag{11}$$

where β_0 is the spanwise wavenumber corresponding to the basic flow periodicity and γ is the detuning parameter, assumed real, which ranges from 0 to 1/2. The modes corresponding to the special values $\gamma = 0$ and $\gamma = 1/2$ are respectively called fundamental and subharmonic. As the basic flow is symmetric about $z = 0$, the modes can be further divided into separate classes according to their odd or even symmetry with respect to the basic flow. In particular, the fundamental modes with an odd symmetry, usually called varicose with reference to their streamline patterns in the (x, z) plane, admit the following expansion:

$$\hat{v}(y,z) = \sum_{k=0}^{\infty} \tilde{v}_k(y)\cos k\beta_0 z; \qquad \hat{\eta}(y,z) = \sum_{k=1}^{\infty} \tilde{\eta}_k(y)\sin k\beta_0 z. \tag{12}$$

The fundamental modes with an even symmetry, usually called sinuous, are of the form

$$\hat{v}(y,z) = \sum_{k=1}^{\infty} \tilde{v}_k(y)\sin k\beta_0 z; \qquad \hat{\eta}(y,z) = \sum_{k=0}^{\infty} \tilde{\eta}_k(y)\cos k\beta_0 z. \tag{13}$$

For subharmonic modes, the same considerations hold, except that the spanwise periodicity of the disturbances is twice that of the basic flow. In this case the odd modes that, by extension, we still call varicose, admit the expansion

$$\hat{v}(y,z) = \sum_{k=0}^{\infty} \tilde{v}_k(y)\cos\left(\frac{k+1}{2}\right)\beta_0 z; \qquad \hat{\eta}(y,z) = \sum_{k=1}^{\infty} \tilde{\eta}_k(y)\sin\left(\frac{k+1}{2}\right)\beta_0 z \tag{14}$$

while the even modes, called sinuous, are expanded according to

$$\hat{v}(y,z) = \sum_{k=1}^{\infty} \tilde{v}_k(y)\sin\left(\frac{k+1}{2}\right)\beta_0 z; \qquad \hat{\eta}(y,z) = \sum_{k=0}^{\infty} \tilde{\eta}_k(y)\cos\left(\frac{k+1}{2}\right)\beta_0 z. \tag{15}$$

Note that spanwise uniform perturbations are considered to be 'fundamental' and are therefore not considered among subharmonic modes. Note also that the 'varicose' ('sinuous') label attributed to the subharmonic odd (even) mode is somehow arbitrary because this mode is varicose (sinuous) with respect to the $z = 0$ axis which we arbitrarily choose in the low speed region of the streak; it would be sinuous (varicose) with respect to the high speed region of the streak.

3.2. Numerical procedure

In order to solve the temporal eigenvalue problem, system (9) and the auxiliary equation (10), are discretised according to the expansions (12), (13) or (14), (15) truncated to N_z terms and Chebyshev expansions truncated to N_y terms are assumed for $\tilde{v}_k(y)$, $\tilde{\eta}_k(y)$ and $\tilde{w}_k(y)$. The semi-infinite y domain is mapped to $(0, L_y)$ through an algebraic transform and the velocity and vorticity fields are evaluated at the Gauss–Lobatto collocation points (see, e.g., Canuto et al. [51]). The results presented in the following have been obtained with $N_y + 1 = 65$ collocation points in the wall normal direction and $N_z = 32$ points in the spanwise direction. Convergence tests were performed on a few selected cases using 97 points in y and 48 in z. For a set of real streamwise wave numbers α at a given Reynolds number R, the complex eigenvalue ω with the largest imaginary part was sought using an implicitly restarted Arnoldi method [52]. The results are considered converged when a relative error below 10^{-9} is attained on the eigenvalues. The used numerical technique is similar to that implemented by Reddy et al. [47], except that the products on the right-hand side of Eqs. (9(a), (b)) are evaluated in physical space and not by convolution in the spanwise spectral space and a different technique is used to sort the leading eigenvalue. The numerical code has been carefully validated in the case of sinuous modes by comparing the results obtained for large amplitude streaks (not discussed in this article) with the inviscid results of Andersson et al. [26] and with those obtained by using the code of Reddy et al. [47] for the same basic flow. In the case of varicose modes, the validation was obtained by recovering standard results for the two-dimensional Blasius profile. We also checked that we obtained the same growth rates as in the direct numerical simulations of the impulse response of the same streaky basic flows performed in CB.

3.3. Production and dissipation of the perturbation kinetic energy

Prandtl [21] used the perturbation kinetic energy equation to gain a physical understanding of the viscous instability mechanism responsible for the destabilisation of TS waves in Blasius profile $U_B(y)$. His rationale was later extended to $U(y, z)$

profiles in the context of the inflectional secondary instability of Görtler vortices (see, e.g., [45,53]). The basic idea is to derive in the usual way the evolution equation for the perturbation kinetic energy density $e' = (u'^2 + v'^2 + w'^2)/2$ from the linearised Navier–Stokes equations (5). Upon integration over a wavelength in the streamwise and spanwise directions and from the wall to infinity in the wall-normal direction, the divergence terms in the evolution equation give a zero global contribution to the energy balance and one is left with

$$\frac{\partial E}{\partial t} = T_y + T_z - D, \tag{16}$$

where the following definitions hold:

$$E = \frac{1}{\lambda_x \lambda_z} \int_0^{\lambda_z} \int_0^{\infty} \int_0^{\lambda_x} e' \,\mathrm{d}x \,\mathrm{d}y \,\mathrm{d}z, \tag{17}$$

$$D = \frac{1}{\lambda_x \lambda_z} \frac{1}{R} \int_0^{\lambda_z} \int_0^{\infty} \int_0^{\lambda_x} \left(\xi'^2 + \eta'^2 + \zeta'^2\right) \mathrm{d}x \,\mathrm{d}y \,\mathrm{d}z, \tag{18}$$

$$T_y = \frac{1}{\lambda_x \lambda_z} \int_0^{\lambda_z} \int_0^{\infty} \int_0^{\lambda_x} (-u'v') \frac{\partial U}{\partial y} \,\mathrm{d}x \,\mathrm{d}y \,\mathrm{d}z, \tag{19}$$

$$T_z = \frac{1}{\lambda_x \lambda_z} \int_0^{\lambda_z} \int_0^{\infty} \int_0^{\lambda_x} (-u'w') \frac{\partial U}{\partial z} \,\mathrm{d}x \,\mathrm{d}y \,\mathrm{d}z. \tag{20}$$

The quantity E is the total perturbation kinetic energy, D is the viscous dissipation term given by the square of the norm of the perturbation vorticity vector (ξ', η', ζ'). T_y and T_z are the perturbation kinetic energy production terms associated with the work of the Reynolds stresses against, respectively, the wall-normal shear $\partial U/\partial y$ and spanwise shear $\partial U/\partial z$. Assuming the normal mode expansion (8) for the perturbations, and upon integration in the streamwise direction, the terms in the energy balance equation are easily seen to be in the form $(E, D, T_y, T_z) = (\widehat{E}, \widehat{D}, \widehat{T}_y, \widehat{T}_z)\,\mathrm{e}^{2\omega_i t}$ with

$$\widehat{E} = \frac{1}{\lambda_z} \int_0^{\lambda_z} \int_0^{\infty} \hat{e} \,\mathrm{d}y \,\mathrm{d}z, \qquad \widehat{D} = \frac{1}{\lambda_z} \int_0^{\lambda_z} \int_0^{\infty} \hat{d} \,\mathrm{d}y \,\mathrm{d}z, \tag{21}$$

$$\widehat{T}_y = \frac{1}{\lambda_z} \int_0^{\lambda_z} \int_0^{\infty} \hat{\tau}_{uv} \frac{\partial U}{\partial y} \,\mathrm{d}y \,\mathrm{d}z, \qquad \widehat{T}_z = \frac{1}{\lambda_z} \int_0^{\lambda_z} \int_0^{\infty} \hat{\tau}_{uw} \frac{\partial U}{\partial z} \,\mathrm{d}y \,\mathrm{d}z, \tag{22}$$

and

$$\hat{e} = (\hat{u}\hat{u}^* + \hat{v}\hat{v}^* + \widehat{w}\widehat{w}^*), \qquad \hat{d} = 2(\hat{\xi}\hat{\xi}^* + \hat{\eta}\hat{\eta}^* + \hat{\zeta}\hat{\zeta}^*)/R,$$
$$\hat{\tau}_{uv} = -(\hat{u}\hat{v}^* + \hat{u}^*\hat{v}), \qquad \hat{\tau}_{uw} = -(\hat{u}\widehat{w}^* + \hat{u}^*\widehat{w}).$$

The following identity is immediately derived from Eq. (16):

$$\omega_i = \frac{\widehat{T}_y}{2\widehat{E}} + \frac{\widehat{T}_z}{2\widehat{E}} - \frac{\widehat{D}}{2\widehat{E}}. \tag{23}$$

In order to evaluate the different terms entering equation (23) one has to know the eigenmode and eigenvalue corresponding to the selected velocity profile $U(y, z)$, Reynolds number R and streamwise wavenumber α. In the absence of errors in the computation, the left-hand side, coming from the eigenvalue computation, and the right-hand side derived from the corresponding mode shape, should match. However, Eq. (23) is more than an a posteriori consistency check of the eigenvalue problem solution, it provides an insight into the viscous instability mechanism by separating the three terms which contribute to the temporal growth rate ω_i. A viscous instability is seen to appear when the work of the Reynolds stresses against the basic shears is able to overcome viscous dissipation. In the following, Eq. (23) will therefore be used to analyse the magnitude of the different physical contributions leading to a given growth rate.

4. Results

4.1. Role of the streak amplitude at a fixed streamwise station and Reynolds number

We begin by investigating the effect of an increasing streak amplitude on the boundary layer stability, keeping fixed the streamwise station X and the Reynolds number. For a set of wave numbers α we compute the eigenvalues having the largest imaginary part ω_i pertaining to the streamwise velocity profiles of the Blasius boundary layer (A) and of the streaks B, C and D prevailing at $X = 2$ (see Table 2). We select $Re_L = 650\,000$ which gives, at $X = 2$, $Re_X = 1\,300\,000$, $R = 1124$ and $R_{\delta^*} = 1934$. All the streaks under consideration are stable to sinuous perturbations. In Fig. 4 we display the temporal growth rate curves $\omega_i(\alpha)$ (on the top row) and the corresponding phase speeds $c_r = \omega_r/\alpha$ (on the bottom row) of varicose perturbations of respectively fundamental (on the left column) and subharmonic type (on the right column). At the Reynolds number under consideration the Blasius boundary layer is unstable. The effect of streaks of increasing amplitude is to reduce the growth rates of fundamental modes (streaks B, C) up to their complete stabilisation for case D. The fundamental modes phase speeds are roughly unchanged with respect to the Blasius-TS waves; they are only slightly reduced as the amplitude and/or wavenumber is increased. The fundamental varicose mode therefore appears to be a sort of 'continuation' of the two-dimensional Blasius-TS waves into three-dimensional streaky-TS waves (see also Ustinov [54]).

Subharmonic modes exhibit growth rates which are an order of magnitude smaller than their fundamental counterparts except for streak D which is stable to fundamental perturbations but is slightly unstable to subharmonic perturbations (this is however a very special case, as will be seen in the following). The subharmonic-mode phase speeds may differ up to 25% from the Blasius-TS phase speeds and they follow an opposite trend since they decrease for increasing wave numbers. The effect of increasing amplitude is not monotone; the low amplitude streak B is stable while streaks C and D are unstable, but streak D is less unstable than streak C.

In Fig. 5 we display the *rms* velocity amplitudes $|\hat{u}(y,z)|$, $|\hat{v}(y,z)|$ and $|\widehat{w}(y,z)|$ of the most unstable varicose fundamental and subharmonic modes of streak C. The contours of the basic flow velocity $U(y,z) = c_r$, corresponding to the phase speed of the mode, and $U(y,z) = 0.99U_\infty$, denoting the boundary layer thickness have also been included for reference. Fundamental and subharmonic modes have quite different structures, but for both, most of the energy is in the streamwise component $\hat{u}$. The fundamental mode displays a $|\hat{u}|$ double-peaked structure concentrated in the low-speed and near the high-speed region: The wall normal profile in the low-speed region has the M-shaped structure observed by Tani and Komoda [17] and Kachanov and Tararykin [18]. The spanwise component $|\widehat{w}|$ is mainly localised in the two regions below the position of maximum spanwise shear $|\partial U/\partial z|$ (see Fig. 3) and attains its maximum amplitude on the line where $U(y,z) = c_r$. The $|\hat{v}|$-component attains its largest values in the low-speed region, it is smaller than $|\hat{u}|$ and it protrudes further away from the wall, as for Blasius-TS waves.

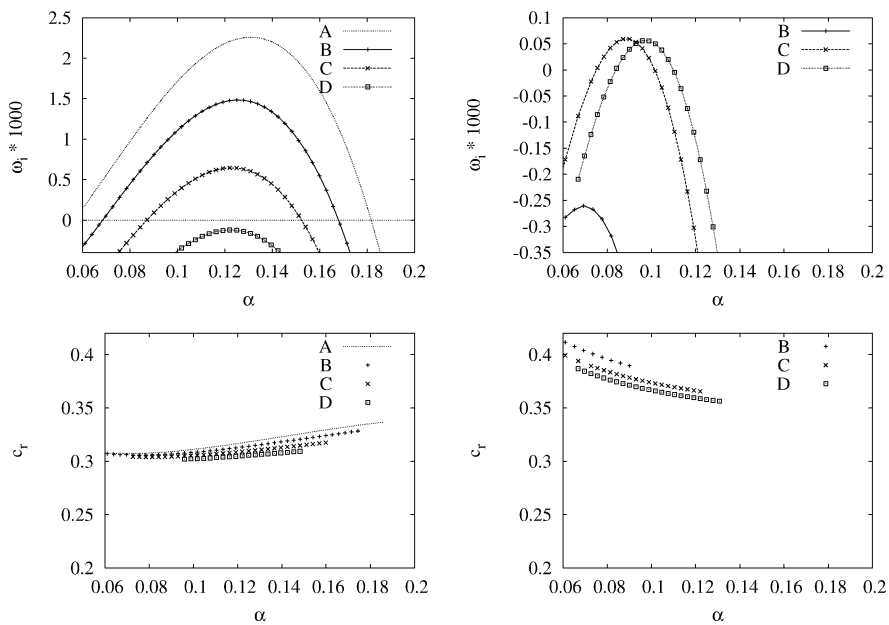

Fig. 4. Growth rate ω_i (top row) and corresponding real phase speed c_r (bottom row) versus streamwise wavenumber α of fundamental (left column) and subharmonic (right column) modes for the Blasius boundary layer A and the streaky flows B, C and D at $X = 2$ for $R = 1124$.

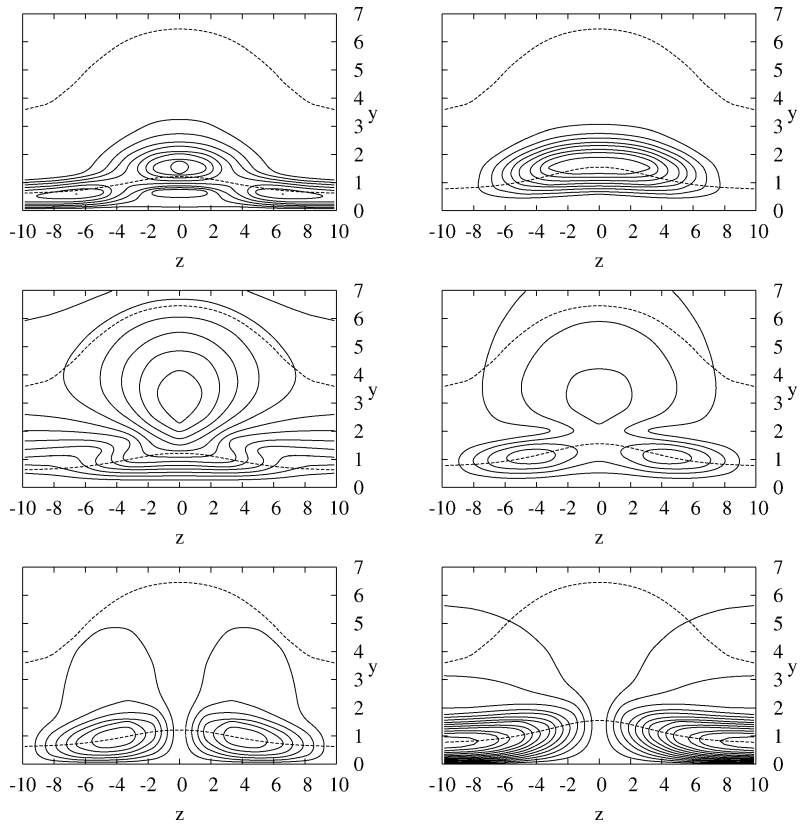

Fig. 5. *Rms* amplitudes of the $\hat{u}(y,z)$ (top), $\hat{v}(y,z)$ (middle) and $\widehat{w}(y,z)$ (bottom) components of the most unstable varicose fundamental (left) and subharmonic (right) modes for the streak C profile extracted at $X=2$ with $R=1124$. The whole mode has been normalised with $\hat{u}_{\max}$ and the contour levels are spaced by $0.1\hat{u}_{\max}$ for $\hat{u}$, $0.01\hat{u}_{\max}$ for $\hat{v}$ and $0.02\hat{u}_{\max}$ for $\widehat{w}$. The maximum contour levels are $0.9\hat{u}_{\max}$ for $\hat{u}$, $0.12\hat{u}_{\max}$ and $0.04\hat{u}_{\max}$ for the wall-normal velocity of the fundamental and subharmonic mode respectively, while the peak contour for the $\widehat{w}$ component has the value $0.12\hat{u}_{\max}$ for the fundamental mode and $0.26\hat{u}_{\max}$ for the subharmonic. The contours $U=c_r$ and $U=0.99U_\infty$ represented by dashed lines of the corresponding basic flows have also been included.

Table 3
Norms of the first spanwise harmonics $\tilde{u}_0(y)$, $\tilde{u}_1(y)$, $\tilde{u}_2(y)$ of the $\hat{u}(y,z)$ most unstable varicose fundamental modes of streaks A, B, C and D with the same parameters as in Figs. 4 and 5

Case	$\|\tilde{u}_0\|$	$\|\tilde{u}_1\|$	$\|\tilde{u}_2\|$
A	1.000	0.000	0.000
B	1.000	0.404	0.157
C	1.000	0.548	0.307
D	1.000	0.628	0.421

The subharmonic mode displays a $|\hat{u}|$ single-peaked structure concentrated in the low-speed region, while $|\widehat{w}|$ is localised in the high-speed region. $|\hat{v}|$ is smaller than $|\hat{u}|$ and $|\widehat{w}|$, it protrudes further away from the wall and has two peaks situated in the flanks of the low-speed region. All the components of the mode reach their maximum amplitude on the $U(y,z)=c_r$ line.

To give an idea of the level of three-dimensionality of the streaky-TS fundamental modes, we document in Table 3 the norms $\|\tilde{u}_k\| = [\int_0^\infty |\tilde{u}_k|^2\,\mathrm{d}y]^{1/2}$ $(k=0,1,2)$ of the spanwise uniform part $\tilde{u}_0$ of the mode and of the first two spanwise harmonics $\tilde{u}_1$ and $\tilde{u}_2$. The most unstable mode of the Blasius profile (case A) is two-dimensional, and therefore there is no energy in the first two spanwise harmonics. For the streaky basic flows, however, the modes are truly three-dimensional: For increasing streak amplitudes, the sum of the energies contained in $\tilde{u}_1$ and $\tilde{u}_2$ may exceed the energy contained in $\tilde{u}_0$. With this in mind we can now analyse the shapes of $|\tilde{u}_0(y)|$, $|\tilde{u}_1(y)|$ and $|\tilde{u}_2(y)|$, plotted in Fig. 6. The spanwise oscillating parts $|\tilde{u}_1(y)|$ and $|\tilde{u}_2(y)|$ keep a fairly constant shape even if their amplitude increases with streak amplitude, as documented above. On the contrary, the

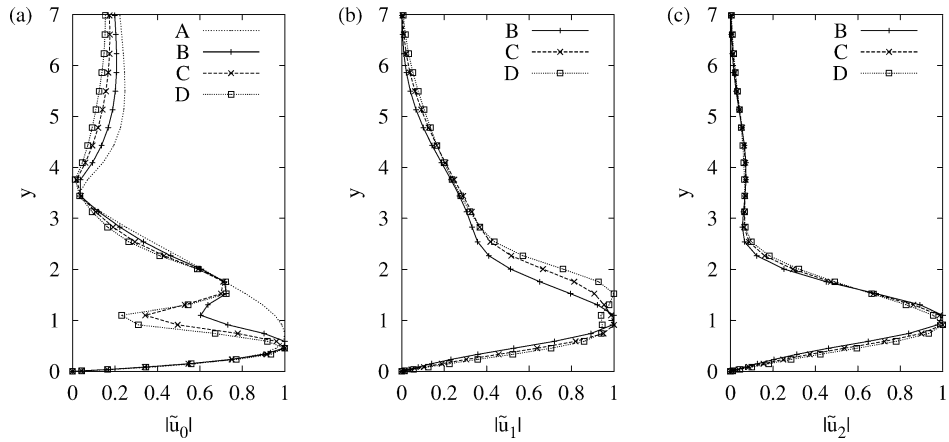

Fig. 6. Wall-normal distribution of: (a) the spanwise independent, (b) the first and (c) the second harmonics of the $\hat{u}$-component for the fundamental varicose modes considered in Fig. 4. The y coordinate is expressed in $\bar{\delta}_X$ units.

spanwise uniform part $|\tilde{u}_0(y)|$ changes its shape. A local 'minimum' appears at the position of maximum amplitude of $|\tilde{u}_1(y)|$ and $|\tilde{u}_2(y)|$. This minimum deepens as the streak amplitude increases. For the streak of largest amplitude a local minimum is seen to appear also in the first harmonic.

4.2. Analysis of the stabilisation mechanism

To gain physical insight into the mechanisms responsible for the observed reduction of the growth rates of the fundamental mode, we report in Table 4 the different terms entering equation (23). These are evaluated for the wave numbers leading to the maximum growth, i.e. at the peak of the $\omega_i(\alpha)$ curves in the top left of Fig. 4. The relative difference between the imaginary part of the computed eigenvalue, on the left-hand side, and the sum of the terms on the right-hand side of (23) was found to be below 4%. The instability of the Blasius boundary layer (case A) must be ascribed, as already well known, to the excess of kinetic energy production T_y, over the viscous dissipation D. As the Blasius profile is two-dimensional, the spanwise shear $\partial U/\partial z$ is zero and therefore there is no contribution from T_z. For streaky flow profiles, however, the term T_z comes into play and it is stabilising. The absolute value of the normalised production and dissipation terms is seen to increase with streak amplitude but the stabilising contribution $(\widehat{T}_z - \widehat{D})/2\widehat{E}$ grows more than the destabilising contribution $\widehat{T}_y/2\widehat{E}$, thereby ultimately leading to stability. The negative production term $\widehat{T}_z/2\widehat{E}$ is of the same order of magnitude as the dissipation term $\widehat{D}/2\widehat{E}$ and therefore it plays an essential role in the stabilisation process. Thus, an asymptotic analysis like the one in Wu and Luo [39] may not be extended to the presently considered streaks. Our results show, in fact, that by not considering the effect of the spanwise shear, streaky-TS waves more unstable than Blasius-TS waves are predicted.

A sample distribution of Reynolds stresses is given in Fig. 7 for the most unstable fundamental mode of streak C. The $\hat{\tau}_{uv}$ term (Fig. 7(a)) is concentrated in the low-speed region of the underlying streak and it is positive, while $\hat{\tau}_{uw}$ (Fig. 7(b)) is localised on the flanks of the low-speed region and it is antisymmetric with respect to the $z = 0$ axis. The distribution of the corresponding induced production terms and of the viscous dissipation term are displayed in Fig. 8. The Reynolds stress $\hat{\tau}_{uv}$ and the wall-normal shear $\partial U/\partial y$ having the same symmetry and the same sign almost everywhere (see Fig. 3), their product gives a dominating positive contribution to T_y (Fig. 8(a)). The kinetic energy production is localised in the low-speed region, as one would also expect from quasi-two-dimensional local analysis. On the other hand, the Reynolds stress $\hat{\tau}_{uw}$ and the spanwise shear $\partial U/\partial z$ have the same symmetry but opposite sign therefore leading to the negative production distribution in Fig. 8(b), and to the stabilising contribution of T_z. The kinetic energy negative production is localised on the flanks of the low-speed

Table 4
Maximum growth rates and normalised kinetic energy production and dissipation components pertaining to the varicose fundamental modes for the streaks considered in Fig. 4

Case	$\omega_{i,\max} \times 10^3$	$\widehat{T}_y/2\widehat{E} \times 10^3$	$\widehat{T}_z/2\widehat{E} \times 10^3$	$\widehat{D}/2\widehat{E} \times 10^3$
A	3.88491213	6.504493	0.	2.617424
B	2.55295653	9.9995469	−2.9446254	4.5003829
C	1.1108635	12.504101	−5.0824684	6.316075
D	−0.209021	13.902289	−6.267457	7.8822505

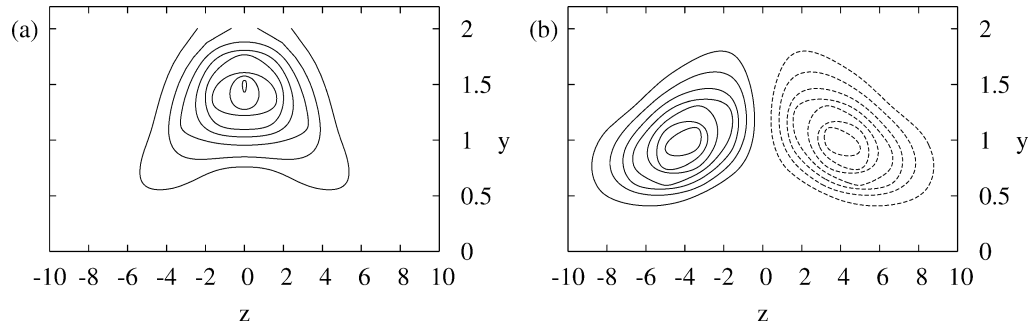

Fig. 7. Normalised Reynolds stresses (a) $\hat{\tau}_{uv}(y,z)/2\widehat{E}$ and (b) $\hat{\tau}_{uw}(y,z)/2\widehat{E}$ pertaining to streak C at $X=2$, $R=1124$, for $\alpha=0.122$. The contour spacing is $0.002\hat{u}_{\max}$. Dashed lines indicate negative values.

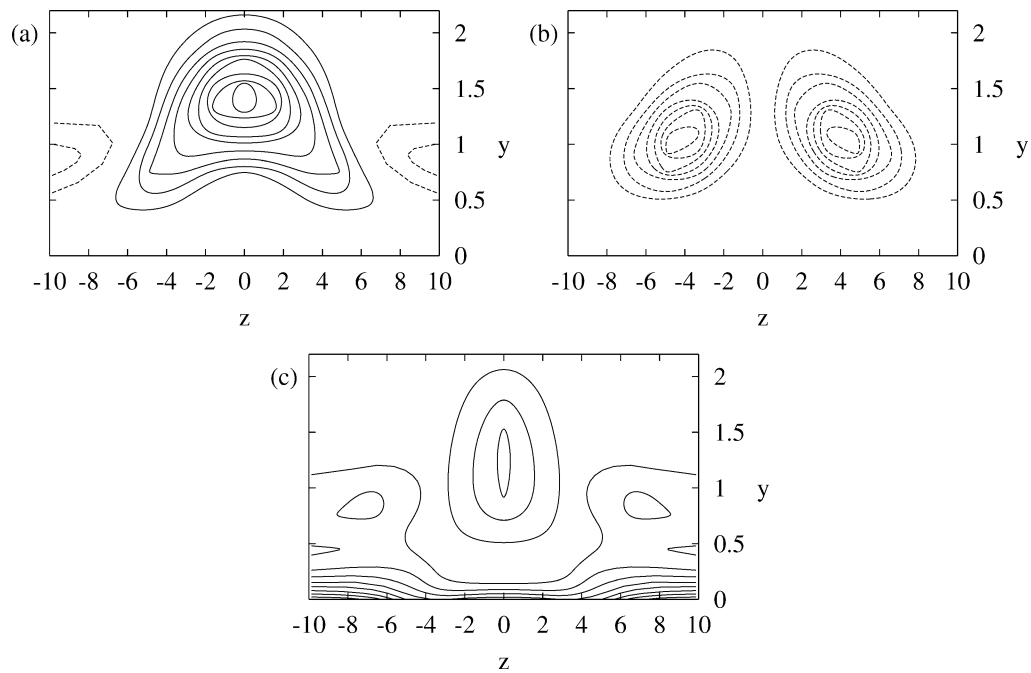

Fig. 8. Normalised production of perturbation kinetic energy: (a) $\hat{\tau}_{uv}(\partial U/\partial y)/|\widehat{T}_y|$, (b) $\hat{\tau}_{uw}(\partial U/\partial z)/|\widehat{T}_z|$, and (c) dissipation $\hat{d}/|\widehat{D}|$ pertaining to most unstable fundamental mode of streak C at $X=2$, $R=1124$, $\alpha=0.122$. The contour spacing is 0.05. Dashed lines indicate negative values.

region and may not be accounted for by quasi-two-dimensional local (in z) analyses. The viscous dissipation, represented in Fig. 8(c), is essentially concentrated very near the wall in the region of highest wall-normal shear. A local maximum of lower intensity can be observed in the low-speed region, in the area of highest positive production.

4.3. Influence of viscosity on the streak temporal stability at fixed streak amplitude and streamwise station

In order to analyse the influence of viscosity on the temporal stability of the streaky boundary layer profiles, we now consider the effect of varying the reference Reynolds number Re_L, and therefore the local Reynolds number R, for a fixed streak amplitude (streak C) at a fixed streamwise station ($X=2$). The increase in R amounts to changing the spanwise scale of the upstream disturbance so that the local spanwise scale prevailing at $X=2$ is attained at increasing distances from the leading edge. Sinuous modes are stable for this profile. The results concerning the varicose modes are presented in Fig. 9, where the curves $\omega_i(\alpha,R)$ of the fundamental (Fig. 9(a)) and subharmonic (Fig. 9(b)) modes are displayed. For the profile under consideration the critical Reynolds number is found to be $R=734$, i.e. more than twice the critical Reynolds number of the Blasius boundary layer in the absence of streaks ($R=304$). The critical mode is the fundamental. Except for a very small

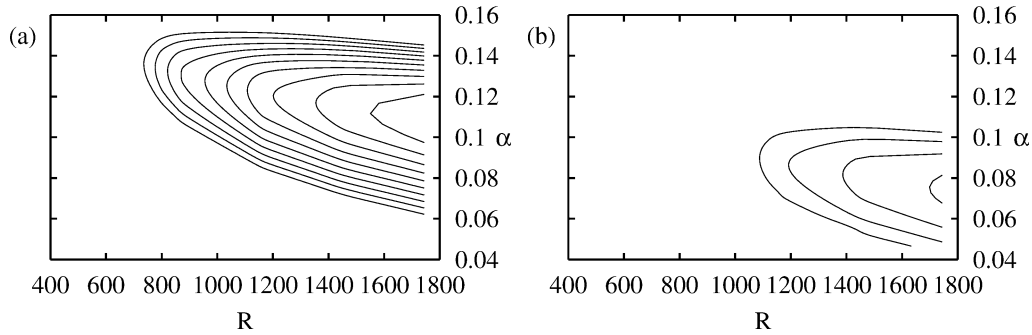

Fig. 9. Growth rate ω_i of the varicose fundamental (a) and subharmonic (b) modes in the streamwise wavenumber α and local Reynolds number R plane for the C streak profile at $X = 2$. Contours start from the neutral curve and proceed, outer to inner, with a spacing of 10^{-4}.

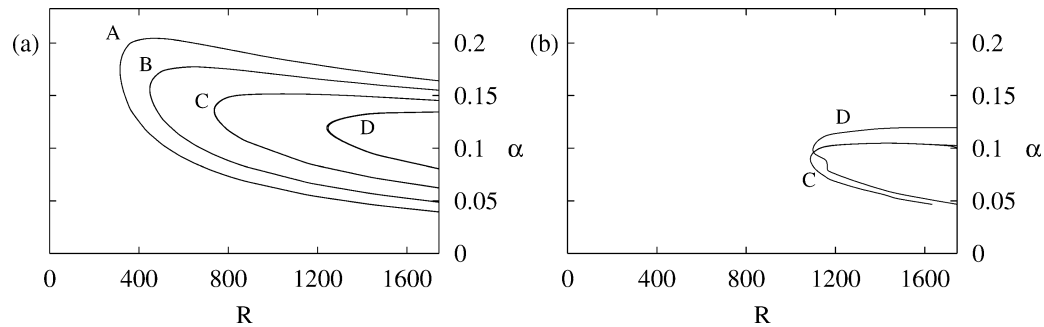

Fig. 10. Neutral stability curves of (a) the fundamental varicose and (b) subharmonic varicose modes as a function of the streamwise wavenumber α and the local Reynolds number R for the Blasius profile (case A) and streaks B, C, and D (outermost to inner curves) extracted at $X = 2$. Subharmonic modes of streak B profiles are stable in the considered Reynolds number range.

region in the parameter plane (roughly $\alpha < 0.07$ and $R > 1100$), the subharmonic varicose modes become unstable at larger Reynolds numbers and their growth rates are smaller than those of the fundamental modes. In principle, intermediate values of the detuning parameter should also be examined. However, previous results (see, e.g., [25,26]) show a monotonic behaviour with the Floquet exponent so that the fundamental and subharmonic modes can be seen as the limiting cases.

To compare the combined effects of viscosity and streak amplitude at fixed X, we repeated the calculations for the other streak profiles at $X = 2$. In Figs. 10(a) and 10(b) we display, respectively, the varicose fundamental and subharmonic neutral curves pertaining to each streak. The effect of increasing streak amplitude is to delay the instability of the fundamental modes, as expected from the results in the previous section (see Fig. 4). The outermost neutral curve shown on the left of Fig. 10 is the well-known neutral curve of the Blasius boundary layer (case A, with a critical Reynolds number $R = 304$). The neutral curves corresponding to streaks of increasing amplitude B, C and D are regularly ordered from outer to inner. The largest amplitude profile, the one corresponding to streak D, is able to delay the instability up to $R \approx 1270$. The amplitude effect on subharmonic modes, as also seen in the previous section, is not monotone; the C and D profiles exhibit essentially the same critical Reynolds number, $R \approx 1100$.

It is important to note that the neutral curves presented in Fig. 10 are *local* neutral curves corresponding to the velocity profiles prevailing at $X = 2$. The variation of $R = Re_X^{1/2} = (XRe_L)^{1/2}$ has been obtained through a variation of Re_L at fixed X, i.e. through a variation of the spanwise scale at the inlet, by exploiting the scaling property introduced in Section 2.

4.4. Stability along the streaky boundary layer

We now consider the stability of a streaky boundary layer by examining the properties of its profiles at different streamwise stations X. For the selected X we choose a range of local Reynolds number R and compute the growth rates $\omega_i(\alpha; R, X)$. The maximum growth rate $\omega_{i,\max}(R, X)$ is obtained by maximising ω_i over α for each R and X. The results pertaining to the varicose modes of streak D, which is the one of largest allowed amplitude before the onset of sinuous inflectional instabilities, are documented in Fig. 11. From the previous sections we know that, for the Reynolds numbers under consideration, the effect of increasing R is destabilising. This is confirmed by the analysis of Fig. 11, where it is seen that, for a constant X, an increase in R leads to instability and then to an increase of the maximum growth rate in the unstable region for both fundamental and

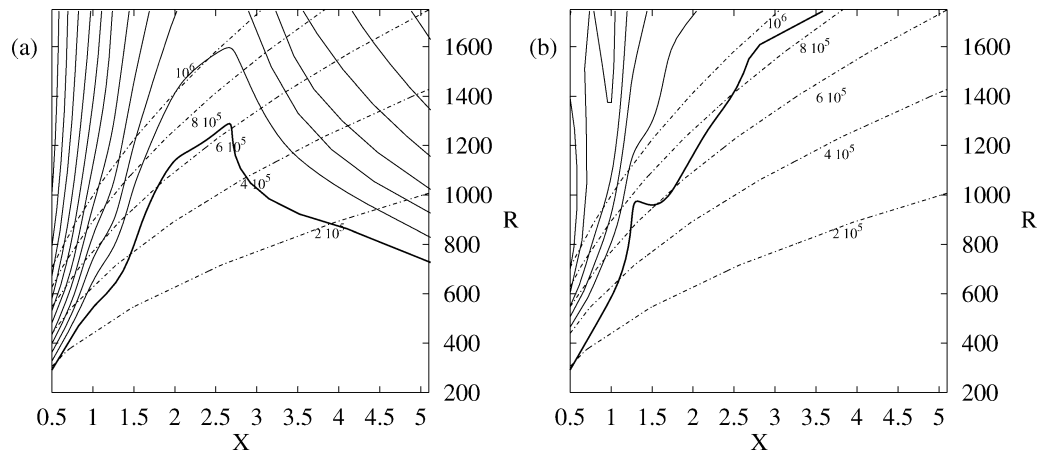

Fig. 11. Maximum growth rate $\omega_{i,\max}$ of (a) varicose fundamental and (b) subharmonic modes pertaining to streak D as a function of streamwise station X and local Reynolds number R. Contour levels are 0 (thick line), 2×10^{-4}, 4×10^{-4}, 6×10^{-4}, ... The dashed lines represent physically realizable streaks at $Re_L = 2\times10^5, 4\times10^5, \ldots, 10^6$.

subharmonic modes. The coordinate X describes the downstream evolution of the streaks and, as a consequence, its effect on the variation of the flow stability features is closely related to the local streak amplitude. Concerning the fundamental modes, we have shown that an increasing streak amplitude is stabilising. The maximum amplitude of streak D is attained roughly at $X = 2$ when T or A_s are used as measures of the streak amplitude and roughly at $X = 2.5$, when E_U is used (see Fig. 1). The former measure seems to better account for the effects of the streak amplitude on the boundary layer stability; in fact, upstream of the peak amplitude ($X < 2.5$), we observe that increasing X at constant R is stabilising since as X increases the streak amplitude also increases. Downstream of the peak amplitude ($X > 2.5$), when X increases the streak amplitude decreases therefore leading to an increase of the growth rates. Subharmonic modes exhibit growth rates generally lower than those of the fundamental modes.

A streaky boundary layer obtained in an experiment or in a numerical simulation sees the same viscosity and free-stream velocity at each streamwise station $\overline{X}$. Physically realizable streaks are therefore obtained at fixed reference Reynolds number Re_L. Along a 'physical streak' the local Reynolds number is given by $R = (Re_L X)^{1/2}$, where Re_L is a constant. To visualise the stability properties of physically realizable streaks, dashed lines corresponding to streaks at $Re_L = 200\,000, 400\,000, \ldots, 1\,000\,000$ are introduced on Fig. 11. As X increases, the local Reynolds number R also increases so that the effects of varying X and R on the stability are coupled. In particular, in the part of the streak which is upstream of its maximum amplitude, the destabilising role of increasing R and the stabilising role of increasing X are in competition. Assuming, for instance, $Re_L = 200\,000$, streak D is stable up to $X = 3.95$, corresponding to $R \approx 880$, to both varicose and subharmonic modes. For $Re_L = 500\,000$ a pocket of instability to both varicose and subharmonic modes appears in the upstream part of the streak (roughly $X < 1.5$) where the streak amplitude is not large enough to counterbalance the destabilising effect of the Reynolds number R. In the range $1.5 < X < 2.7$ the stabilising effect of the streak amplitude dominates, but eventually, for $X > 2.7$, at roughly $R = 1160$, fundamental modes become unstable again.

The computations have been repeated for the others streaky basic flows; the corresponding neutral curves are displayed in Fig. 12. As expected, streak D is the most effective in delaying the instability. The fundamental-mode neutral curve for the lowest amplitude streak is very close to the neutral curve of the Blasius boundary layer, which becomes unstable at $R = 304$ for all X. It can be seen that for all the streaks under consideration the maximum amplitude profile, prevailing at $X \approx 2.5$, may be stable for quite large values of R (e.g. $R = 1270$ for streak D). However, the stability of a physically realizable streak, obtained following one of the dashed lines in the plot, may be obtained only up to lower R values (e.g. $R = 880$ for streak D) because in the upstream part of the streak the amplitude is not large enough to counterbalance the destabilising increase of R. This effect is particularly strong for the streaks we consider here because, as their growth is optimised, they have, upstream of their peak value, amplitudes that are generally lower than for other possible non-optimal streaks. It should in fact be observed that if the upstream vortices are induced using wall-roughness elements or blowing-suction slots, their amplitude evolution would not be the same as for the optimal perturbations used here (see, e.g., [20]).

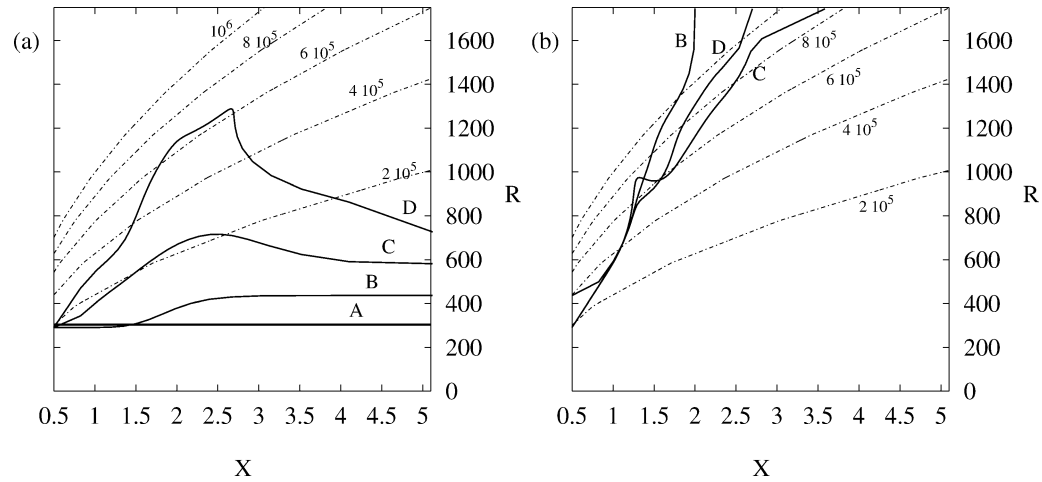

Fig. 12. Neutral stability curves for (a) fundamental varicose and (b) subharmonic varicose modes for the Blasius boundary layer A and the streaks B, C and D as a function of streamwise station X and local Reynolds number R. The dashed lines represent physically realizable streaks at $Re_L = 2 \times 10^5, 4 \times 10^5, \ldots, 10^6$.

4.5. Implications for transition delay

Most of 'open-loop' transition delay methods rely on the suppression or reduction of the exponential growth of the unstable waves in the linear regime, obtained for instance by enforcing favourable pressure gradients, through wall suction, fluid heating or cooling, etc. The forcing of steady streaks in a flat plate boundary layer might be as effective as other methods in delaying transition. A clear advantage of this scheme is the fact that the 'actuators' modifying the basic flow stability behaviour can be placed upstream of the unstable region and presumably require little energy because the streak extracts its energy from the basic flow itself through the 'lift-up' effect. In the previous section we have shown that for streak D it is possible to delay the onset of instability up to R above 850 (corresponding to R_{δ^*} above 1450 and Re_X above 720 000) by choosing $Re_L = 200\,000$. For largest Re_L a pocket of instability appears in the upstream part of the streak, which is however followed by a large region of stable flow.

To allow a quantitative comparison with other transition delay methods, the computation of spatial growth rates would be necessary to estimate the total growths at fixed real frequency (the so called n-factors used in the e^N method). Further, a complete analysis of the possible transition delay would also require a parametric study of the spanwise wavenumber β of the streaks. The wavelength of optimal spatial growth is not necessarily optimal for the stabilisation process investigated here, and, in fact, one may expect that streaks of larger wave numbers, thus associated with stronger spanwise gradients, have a stronger stabilising effect. Such a parametric study is not attempted in this article since the computation of a number of streaky boundary layers with different spanwise wave numbers and amplitudes is still a formidable task. The aim of the paper is to show the high potentiality of spanwise modulated flows to delay viscous instabilities and give a physical explanation for it. We believe that an experimental study is now more adequate to explore the effect of the wavenumber β and estimate the spatial growth rate reductions.

However, by considering the temporal growth rates and computing the group velocities from the results obtained (see Fig. 4), it is possible, using Gaster's transformation, to roughly estimate the spatial growth rates from the temporal results [55]. It can be shown that large reductions of the growth rates are attained both in the pocket of instability observed at low X and downstream of the neutral curves. For the fundamental varicose instability, the estimated growth rates are less than half of those pertaining to the two-dimensional boundary layer, while the growth rates of the subharmonic modes are about 1% of those of the Blasius profile.

To evaluate the performance of the proposed control strategy one must also evaluate the energy used in the generation of the streaks and the energy loss due to the presence of the streaks in the boundary layer. No external energy is needed to generate the streaks if passive methods, like vortex generators or roughness elements, are used. If instead the streaks are induced by active methods, like blowing and suction at the wall, the energy used can still be considered negligible because the 'lift-up' effect acts as an amplifier of the actuator energy. Typically the lift-up gain is of order Re_X in the linear approximation. On the other hand, the skin friction coefficient C_f pertaining to the B, C and D basic flows is larger than that of the Blasius two-dimensional boundary layer. The C_f increase is due to the spanwise uniform part of the basic flow distortion induced by the streaks through nonlinear effects. These lead to 'fuller' velocity profiles (see CB) and to larger shear at the wall. On Fig. 13 we display the

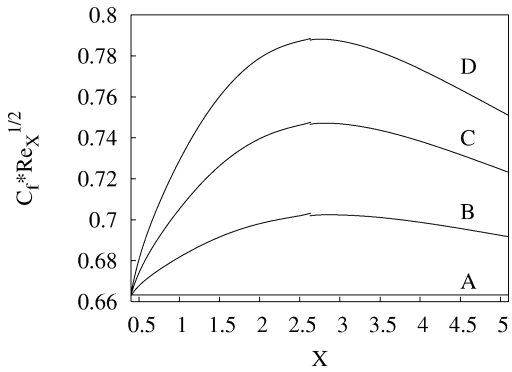

Fig. 13. Streamwise evolution of normalised skin friction coefficient $C_f Re_X^{1/2}$ for the Blasius boundary layer A and for streaky boundary layers B, C and D.

streamwise evolution of normalised skin friction coefficient $C_f Re_X^{1/2}$ for the Blasius boundary layer A and the streaks under consideration. The skin friction coefficient increases at worst by less than 20% when compared to the Blasius case.

5. Conclusions

The linear viscous stability of the boundary layer on a flat plate in the presence of nonlinear streamwise streaks assumed steady and spanwise periodic has been analysed by means of Floquet theory. The main results of the present study can be summarised as follows.

The most unstable waves are modified by the presence of the streaks: They evolve from two-dimensional TS waves into three-dimensional varicose fundamental modes, here called 'streaky-TS waves'. The latter have almost identical phase speed but lower growth rates than the TS waves and a characteristic M-shaped structure of their *rms* streamwise velocity amplitude. These results are in agreement with previous experimental investigations (cf. [17,18]).

The analysis of the growth rates of the streaky-TS waves confirms the stabilising effect of steady streaks on the viscous instability [18,41] and that this stabilising effect increases with the streak amplitude.

A physical explanation for the observed stabilisation is provided by considering the kinetic energy production for the most unstable waves. The viscous instability is, in the presence of the streaks, fed by the work of the uv-Reynolds stress against the wall normal shear $\partial U/\partial y$, just as in the two-dimensional boundary layer. However, the work of the uw-Reynolds stresses against the spanwise shear $\partial U/\partial z$ is stabilising. This stabilising contribution and the viscous dissipation increase with the streak amplitude, thereby reducing the growth rate and eventually leading to stability.

Results for the varicose subharmonic modes are presented: these modes are also found to be unstable but they have growth rates which typically are an order of magnitude lower than those of fundamental modes. For the family of intermediate-amplitude streaks considered in the present study, sinuous modes are always stable.

The possible relevance of streak stabilisation for applications in boundary layer transition delay has also been discussed. The efficiency of the generation of the streaks, the fact that the actuators do not need to cover all the unstable domain, and the large displacement of the neutral stability curves are seen as very promising trends. A similar control strategy has been suggested in order to delay cross-flow instability in swept wing boundary layers [56,57].

Our results may probably be related also to the observed average reduction of the growth of small amplitude TS waves developing in a boundary layer exposed to free-stream turbulence [38]. In this case however, the streaks are unsteady, so that further investigations seem necessary in order to assess the importance of this additional factor and whether the stabilising effect of steady streaks can contrast the destibilising effect of free-stream turbulence.

Acknowledgements

We kindly acknowledge P. Huerre and D.S. Henningson for their useful remarks on the manuscript and S. Reddy for providing the stability code which was used to validate our numerical method. Part of the computational facilities were provided by CNRS/IDRIS. LB acknowledges financial support by VR (Vetenskapsrådet) and by École Polytechnique during his stay at LadHyX.

References

[1] H. Schlichting, Boundary-Layer Theory, McGraw-Hill, New York, 1979.
[2] M.T. Landahl, Wave breakdown and turbulence, SIAM J. Appl. Math. 28 (1975) 735–756.
[3] T. Ellingsen, E. Palm, Stability of linear flow, Phys. Fluids 18 (1975) 487–488.
[4] L.H. Gustavsson, Energy growth of three-dimensional disturbances in plane Poiseuille flow, J. Fluid Mech. 224 (1991) 241–260.
[5] S.C. Reddy, D.S. Henningson, Energy growth in viscous channel flows, J. Fluid Mech. 252 (1993) 209–238.
[6] P.J. Schmid, D.S. Henningson, Stability and Transition in Shear Flows, Springer, New York, 2001.
[7] P. Andersson, M. Berggren, D.S. Henningson, Optimal disturbances and bypass transition in boundary layers, Phys. Fluids 11 (1999) 134–150.
[8] P. Luchini, Reynolds-number independent instability of the boundary layer over a flat surface. Part 2: Optimal perturbations, J. Fluid Mech. 404 (2000) 289–309.
[9] M. Choudhari, Boundary-layer receptivity to three-dimensional unstaedy vortical disturbances in the free stream, AIAA Paper 96, 0181, 1996.
[10] F.P. Bertolotti, Response of the Blasius boundary layer to free-stream vorticity, Phys. Fluids 9 (8) (1997) 2286–2299.
[11] D.W. Wundrow, M.E. Goldstein, Effect on a laminar boundary layer of small-amplitude streamwise vorticity in the upstream flow, J. Fluid Mech. 426 (2001) 229–262.
[12] H.L. Dryden, Air flow in the boundary layer near a plate. Report 562, NACA, 1937.
[13] G.I. Taylor, Some recent developments in the study of turbulence, in: J. Hartog, H. Peters (Eds.), Proc. 5th Int. Congr. Appl. Mech., Wiley, 1939, pp. 294–310.
[14] D. Arnal, J.C. Juillen, Contribution expérimentale à l'étude de la reptivité d'une couche limite laminaire à la turbulence de l'écoulement général, Rapport Technique 1/5018, ONERA, 1978.
[15] J.M. Kendall, Experimental study of disturbances produced in a pre-transitional laminar boundary layer by weak free-stream turbulence, AIAA Paper 85 (1985) 1695.
[16] P.S. Klebanoff, Effect of free-stream turbulence on the laminar boundary layer, Bull. Am. Phys. Soc. 10 (1971) 1323.
[17] I. Tani, H. Komoda, Boundary layer transition in the presence of streamwise vortices, J. Aerospace Sci. 29 (1962) 440.
[18] Y.S. Kachanov, O.I. Tararykin, Experimental investigation of a relaxating boundary layer, Izv. SO AN SSSR Ser. Tech. Nauk 18 (1987).
[19] A.A. Bakchinov, G.R. Grek, B.G.B. Klingmann, V.V. Kozlov, Transition experiments in a boundary layer with embedded streamwise vortices, Phys. Fluids 7 (1995) 820–832.
[20] E.B. White, Transient growth of stationary disturbances in a flat plate boundary layer, Phys. Fluids 14 (2002) 4429–4439.
[21] L. Prandtl, Bemerkungen über die Enstehung der Turbulenz, ZAMM 1 (1921) 431–435.
[22] W. Tollmien, Über die Entstehung der Turbulenz, Nachr. Ges. Wiss. Göttingen 21–24 (1929). English translation NACA TM 609, 1931.
[23] H. Schlichting, Berechnung der Anfachung kleiner Störungen bei der Plattenströmung, ZAMM 13 (1933) 171–174.
[24] G.B. Schubauer, H.F. Skramstad, Laminar boundary layer oscillations and the stability of laminar flow, J. Aero. Sci. 14 (1947) 69–78.
[25] T. Herbert, Secondary instability of boundary-layers, Annu. Rev. Fluid Mech. 20 (1988) 487–526.
[26] P. Andersson, L. Brandt, A. Bottaro, D.S. Henningson, On the breakdown of boundary layers streaks, J. Fluid Mech. 428 (2001) 29–60.
[27] L. Brandt, D.S. Henningson, Transition of streamwise streaks in zero-pressure-gradient boundary layers, J. Fluid Mech. 472 (2002) 229–262.
[28] M. Matsubara, P.H. Alfredsson, Disturbance growth in boundary layers subjected to free stream turbulence, J. Fluid. Mech. 430 (2001) 149–168.
[29] R.G. Jacobs, P.A. Durbin, Simulations of bypass transition, J. Fluid Mech. 428 (2001) 185–212.
[30] W. Schoppa, F. Hussain, Coherent structure generation in near-wall turbulence, J. Fluid Mech. 453 (2002) 57–108.
[31] L. Brandt, P. Schlatter, D.S. Henningson, Numerical simulations of transition in a boundary layer under free-stream turbulence, in: I. Castro, P.E.H. Thomas (Eds.), Advances in Turbulence IX, Proc. of the Ninth European Turbulence Conference, Springer, 2002, pp. 17–20.
[32] L. Brandt, Numerical studies of bypass transition in the Blasius boundary layer. Ph.D. thesis, Royal Institute of Technology, Stockholm, Sweden, 2003.
[33] M. Asai, M. Minagawa, M. Nishioka, The instability and breakdown of a near-wall low-speed streak, J. Fluid Mech. 455 (2002) 289–314.
[34] X. Wu, M. Choudhari, Linear and nonlinear instabilities of a Blasius boundary layer perturbed by streamwise vortices. Part II: Intermittent instability induced by long-wavelength Klebanoff modes, J. Fluid Mech. 483 (2003) 249–286.
[35] H.L. Reed, W.S. Saric, Stability of three-dimensional boundary layers, Annu. Rev. Fluid Mech. 21 (1989) 235–284.
[36] H. Komoda, Nonlinear development of disturbance in a laminar boundary layer, Phys. Fluids Suppl. 10 (1967) S87.
[37] H.R. Grek, V.V. Koslov, M.P. Ramazanov, Investigation of boundary layer stability in the presence of high degree of free-stream turbulence, in: Proc. of Int. Seminar of Problems of Wind Tunnel Modeling, vol. 1, Novosibirsk, 1989 (in Russian).
[38] A.V. Boiko, K.J.A. Westin, B.G.B. Klingmann, V.V. Kozlov, P.H. Alfredsson, Experiments in a boundary layer subjected to free stream turbulence. Part 2. The role of TS-waves in the transition process, J. Fluid Mech. 281 (1994) 219–245.
[39] X. Wu, J. Luo, Linear and nonlinear instabilities of a Blasius boundary layer perturbed by streamwise vortices. Part 1. Steady streaks, J. Fluid Mech. 483 (2003) 225–248.
[40] M.E. Goldstein, D.W. Wundrow, Interaction of oblique instability waves with weak streamwise vortices, J. Fluid Mech. 284 (1995) 377–407.
[41] C. Cossu, L. Brandt, Stabilization of Tollmien–Schlichting waves by finite amplitude optimal streaks in the Blasius boundary layer, Phys. Fluids 14 (2002) L57–L60.

[42] M.N. Kogan, M.V. Ustinov, Boundary layer stabilization by “artificial turbulence”, Fluid Dynamics 38 (2003) 571–580.
[43] P. Hall, N.J. Horseman, The linear inviscid secondary instability of longitudinal vortex structures in boundary-layers, J. Fluid Mech. 232 (1991) 357–375.
[44] X. Yu, J. Liu, On the secondary instability in Goertler flow, Phys. Fluids A 3 (1991) 1845.
[45] X. Yu, J. Liu, On the mechanism of sinuous and varicose modes in three-dimensional viscous secondary instability of nonlinear Görtler rolls, Phys. Fluids 6 (2) (1994) 736–750.
[46] F. Waleffe, Hydrodynamic stability and turbulence: beyond transients to a self-sustaining process, Stud. Appl. Math. 95 (1995) 319–343.
[47] S.C. Reddy, P.J. Schmid, J.S. Baggett, D.S. Henningson, On the stability of streamwise streaks and transition thresholds in plane channel flows, J. Fluid Mech. 365 (1998) 269–303.
[48] A. Lundbladh, S. Berlin, M. Skote, C. Hildings, J. Choi, J. Kim, D.S. Henningson, An efficient spectral method for simulation of incompressible flow over a flat plate, Technical Report KTH/MEK/TR-99/11-SE, KTH, Department of Mechanics, Stockholm, 1999.
[49] L. Brandt, C. Cossu, J.-M. Chomaz, P. Huerre, D.S. Henningson, On the convectively unstable nature of optimal streaks in boundary layers, J. Fluid Mech. 485 (2003) 221–242.
[50] P. Drazin, W. Reid, Hydrodynamic Stability, Cambridge Univ. Press, 1981.
[51] C. Canuto, Y.M. Hussaini, A. Quarteroni, T.A. Zang, Spectral Methods in Fluid Dynamics, Springer, New York, 1988.
[52] R.B. Lehoucq, D.C. Sorensen, C. Yang, ARPACK user guide: Solution of Large-Scale Eigenvalue Problems with Implicitly Restarted Arnoldi Methods, SIAM, Philadelphia, 1998.
[53] D.S. Park, P. Huerre, Primary and secondary instabilities of the asymptotic suction boundary layer on a curved plate, J. Fluid Mech. 283 (1995) 249–272.
[54] M.V. Ustinov, Stability of the flow in a streaky structure and the development of perturbations generated by a point source inside it, Fluid Dynamics 37 (2002) 9–20.
[55] M. Gaster, A note on the relation between temporally-increasing and spatially-increasing disturbances in hydrodynamic stability, J. Fluid Mech. 14 (14) (1962) 222–224.
[56] W.S. Saric, R.B. Carrillo Jr., M.S. Reibert, Leading-edge roughness as a transition control mechanism, AIAA Paper-98-0781, 1998.
[57] P. Wassermann, M. Kloker, Mechanisms and passive control of crossflow-vortex-induced transition in a three-dimensional boundary layer, J. Fluid Mech. 456 (2002) 49–84.